参赛学生姓名： 王雪扬

中学： 四川大学附属中学

省份： 四川省

国家/地区： 中国

指导老师姓名： 巨晓洁、何春燕

指导老师单位： 四川大学化学工程学院、四川大学附中

论文题目： 共载一氧化氮供体和米诺地尔的增发微针的研究

Nitric Oxide Donor and Minoxidil Co-loaded Microneedles Improve Hair Loss Treatment

Participant

Xueyang Wang

School

The Affiliated High School of Sichuan University

Location

Chengdu, Sichuan, P.R. China

Instructor

Xiaojie Ju

(The School of Chemical Engineering, Sichuan University)

Chunyan He

(The Affiliated High School of Sichuan University)

Contents

Catalog

Abstract

Currently, the treatment of androgenetic alopecia (AGA) is mostly achieved by local application of minoxidil tincture. But there are significant limitations, including ineffectiveness on its own, poor patient compliance and low transdermal absorption. Microneedles (MNs) can puncture the stratum corneum without pain and increase the absorption of drugs through the skin. Additionally, nitric oxide (NO) has been shown to improve blood supply to hair follicles and reduce inflammation. Therefore, we prepared a kind of hair-growth microneedles, which can co-deliver minoxidil and NO donor for AGA treatment. In simple terms, the nanogel (MHMA) was formed through photopolymerization of and methacryloyl hyaluronic acid (MeHA) and the NO donor methacryloyl arginine (MeArg). Through optimized formulation design, minoxidil was efficiently encapsulated within the nanogel (MHMA) with a particle size of 522.9 nanometer，which will facilitate its targeting to hair follicles. Subsequently, the microneedles were prepared using a micro-molding method. Both in vitro and in vivo experiments demonstrated that the hair growth-promoting microneedles could efficiently deliver minoxidil and NO donor with just 3 minutes pressing on mouse skin. It effectively promoted the transition of hair follicles into the growth phase and stimulated angiogenesis around the follicles, ultimately leading to hair regeneration in a mouse model of hair loss. Overall, the hair growth microneedles efficiently deliver minoxidil and NO donor into skin without pain, thus offering a promising new direction for clinical AGA treatment.

摘 要

目前，雄激素性脱发（AGA）的治疗主要依赖于局部应用米诺地尔酊剂。但这种方法存在明显的局限，如疗效不佳、患者依从性差和药物透皮吸收效率低等问题。微针（MNs）技术能无痛地穿透皮肤角质层，从而增加药物的经皮吸收。此外，一氧化氮（NO）已被证明可以改善毛囊部位的血流供应和减少炎症。因此，我们开发了一种新型的增发微针，期望实现米诺地尔和 NO 供体的共递送。具体而言，首先通过光聚合反应制备纳米凝胶（MHMA），它是由甲基丙烯酰基透明质酸（MeHA）和 NO 的供体甲基丙烯酰基精氨酸（MeArg）聚合而成。通过优化配方设计，米诺地尔被高效地包封在纳米凝胶（MHMA）中，其粒径为 522.9 nm，这有利于实现毛囊细胞的靶向。随后，采用微模板法制备了微针。体外和体内实验表明，这种增发微针在小鼠皮肤上按压 3 分钟即可实现米诺地尔和 NO 供体的高效递送；它能够有效促进毛囊进入生长期，刺激毛囊周围的血管生成，并在脱发的小鼠模型中实现毛发再生。总体而言，这种生发微针能够高效、无痛地将米诺地尔和 NO 供体递送至皮肤中，实现 NO 与米诺地尔的协同治疗，为临床 AGA 的治疗提供了有前景的新方向。

Body Text

1 Introduction

Androgenetic Alopecia (AGA) is currently the most common type of hair loss seen in clinical settings[1, 2]. In China, epidemiological data indicates that the prevalence of male AGA is 21.3%, while for females, it is 6.0%[3]. The main characteristics of AGA include follicular miniaturization, hair thinning, and excessive shedding, which significantly impact patients' quality of life and mental health. Although the molecular pathogenesis of AGA is not fully understood, studies have shown that increased levels of dihydrotestosterone (DHT) and androgen receptors (AR) are closely associated with the onset of AGA [4]. DHT is converted from testosterone via 5-alpha-reductase and has about 10 times the androgenic activity of testosterone. In hair follicles, DHT forms dimers with AR proteins in the cytoplasm of dermal papilla cells, which are then transported to the nucleus to act as transcription factors, promoting the expression of hair growth-inhibitory proteins (such as TGF-β and DKK-1), leading to follicular aging and degradation. Additionally, the Wnt/β-Catenin signaling pathway plays a key role in the early morphogenesis, development, and regeneration of hair follicles during the hair cycle[5]. Inhibition of Wnt signaling may be associated with abnormal hair reduction. Oxidative stress in the microenvironment surrounding the hair follicle is another possible factor in hair loss. Excessive reactive oxygen species (ROS) can mediate androgen signaling and may also induce premature aging of dermal papilla cells, while simultaneously inhibiting angiogenesis, leading to vascular dysfunction and preventing the transition of hair follicles from the resting phase to the growth phase[6].

The most common clinical treatment for AGA is topical application of minoxidil, which is currently recognized as an effective anti-hair loss treatment worldwide. Minoxidil prevents hair loss and promotes hair growth through multiple mechanisms: (1) directly stimulating the proliferation and differentiation of follicular epithelial cells; (2) promoting angiogenesis, increasing local blood supply, and dilating scalp blood vessels; (3) activating the WNT/β-catenin signaling pathway to promote the growth and development of hair follicles; (4) regulating the hair growth cycle, causing more hair follicles to transition from the resting phase to the growth phase[7, 8]. However, due to the poor solubility of minoxidil, it is mainly available in a tincture form, using ethanol or propylene glycol as solvents. Organic solvents are volatile, leading to crystallization of the drug on the skin surface, which hinders absorption. Moreover, long-term use of organic solvents can irritate the skin, causing oily hair, rapid hair loss, dermatitis, and allergic reactions, and may even lead to hypotension and tachycardia[9].

Other studies have reported that insufficient vascularization in the hair loss areas of AGA patients can hinder the delivery of active nutrients and therapeutic drugs like minoxidil to the follicles, significantly reducing minoxidil's bioavailability. As a result, the efficacy of minoxidil is greatly

diminished, requiring patients to use the drug frequently over long periods, which significantly decrease patient adherence[9]. In recent years, the role of nitric oxide (NO) in promoting hair growth has gradually gained attention among researchers[10]. NO can indeed play a synergistic role in minoxidil treatment for AGA through several mechanisms: 1) Vasodilation and increased blood flow, enhancing drug penetration; 2) Promoting neovascularization; 3) Accelerating proliferation and migration of dermal papilla cells; 4) Reducing inflammatory immune responses[11]. The most widely studied nitric oxide donors include organic nitrates (RONO2), nitrites (RONO), S-nitrosothiols (RSNO), nitrosamines, N-diazeniumdiolate salts (NONOates), and metal-NO complexes[10-12]. Among them, RSNO and NONOates are the two most widely used NO donors. Although these NO donors are more stable than NO gas and can be stored as solids, they still have short half-lives, low bioavailability, and poor stabilities. L-arginine, an endogenous amino acid, can be metabolized to NO and L-citrulline under the action of nitric oxide synthase (NOS) or ROS. More importantly, compared with RSNO and NONOates, L-arginine has much better biocompatibility, stability, and druggability[13, 14]. Currently, oral and injectable L-arginine medications are available in clinical practice. Therefore, exploring L-arginine as a NO donor to improve insufficient vascularization in hair loss areas, in combination with minoxidil, holds promising clinical potential for the treatment of AGA.

Microneedles (MNs) are micron-scaled tiny needles measuring 100 to 1000 μm. They are designed for minimally invasive and nearly painless penetration of the stratum corneum, the outermost layer of the skin. Compared to topical formulations like minoxidil tincture, microneedles can deliver drugs more efficiently into the skin (**Scheme 1**). This technology addresses the challenges of low transdermal efficiency and poor compliance often associated with AGA treatments[15, 16].

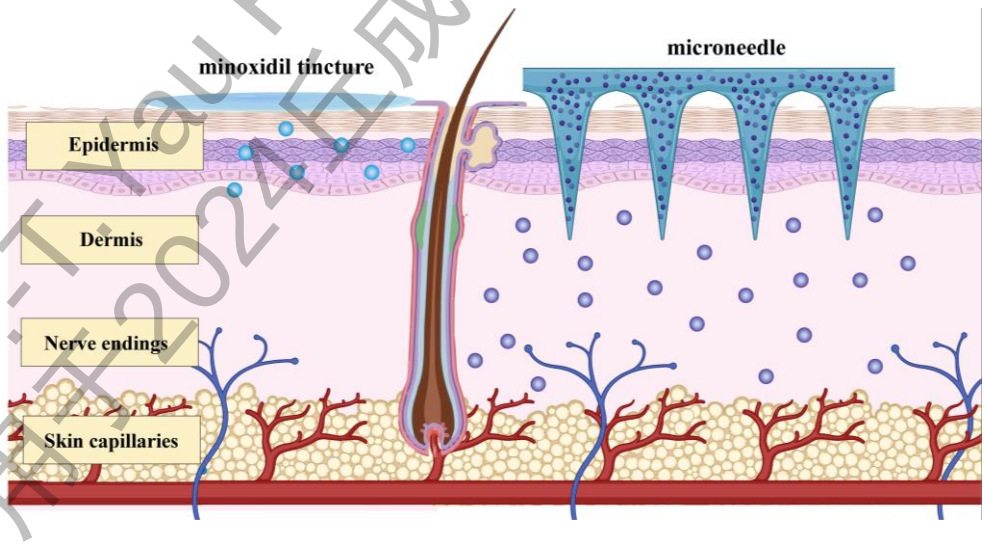

Scheme 1 Microneedles (MN) are micron-sized needles designed to minimally invasively and painlessly penetrate the stratum corneum, facilitating more efficient drug delivery into the skin compared to minoxidil tincture.

Additionally, the rapid advancement of nanotechnology has opened new opportunities for hair follicle regeneration. By designing nanoparticles with specific characteristics, researchers can achieve targeted drug delivery to hair follicles, allowing drugs to penetrate deeply into the follicle roots for more effective treatment[17, 18]. It has been indicated in literature that nanoparticles with diameters ranging from 400 nm to 600 nm show deeper penetration within hair follicles[19, 20]. This targeted delivery strategy not only improves treatment efficacy but also minimizes side effects, providing significant benefits for patients suffering from hair loss.

Based on the above background, this study designed a novel drug delivery system for AGA treatment, utilizing microneedles as a delivery platform to efficiently co-deliver minoxidil and NO donors in a nano-hydrogel. Specifically, the nano-hydrogel (MHMA) was formed by photopolymerization of Methacryloyl hyaluronic acid (MeHA) and Methacryloyl arginine (MeArg), with MeArg serving as the NO donor. Through optimized formulation design, this nano-hydrogel efficiently encapsulated minoxidil (MI) in a non-organic solvent, resulting in a drug-loaded nano-hydrogel co-encapsulating arginine and minoxidil (MHMA@MI). Furthermore, using a micro-molding method, MHMA@MI was loaded into microneedles to produce hair-growth microneedles (MN-MHMA@MI) (**Scheme 2**). The prepared hair-growth microneedles demonstrated complete morphological structure and excellent mechanical properties, successfully penetrating the stratum corneum and effectively delivering MHMA@MI into the skin. Compared to commercially available minoxidil tincture and minoxidil microneedles (MN-MI), MN-MHMA@MI showed the most significant hair regeneration effect in a mouse hair loss model. Hematoxylin-Eosin staining (H&E) results demonstrated that MN-MHMA@MI effectively promoted hair follicles to enter the growth phase. Meanwhile, CD31 immunofluorescence staining results indicated that the MN-MHMA@MI group stimulated angiogenesis around the hair follicles and improved blood supply to the follicles. In addition, the microneedles were free of organic solvents, and no significant damage was observed in the skin tissue during the treating period, confirming the excellent biosafety of MN-MHMA@MI. Therefore, the hair-growth microneedles we developed highlight their potential as a safe and effective treatment for AGA, further supporting their potentials in clinical application.

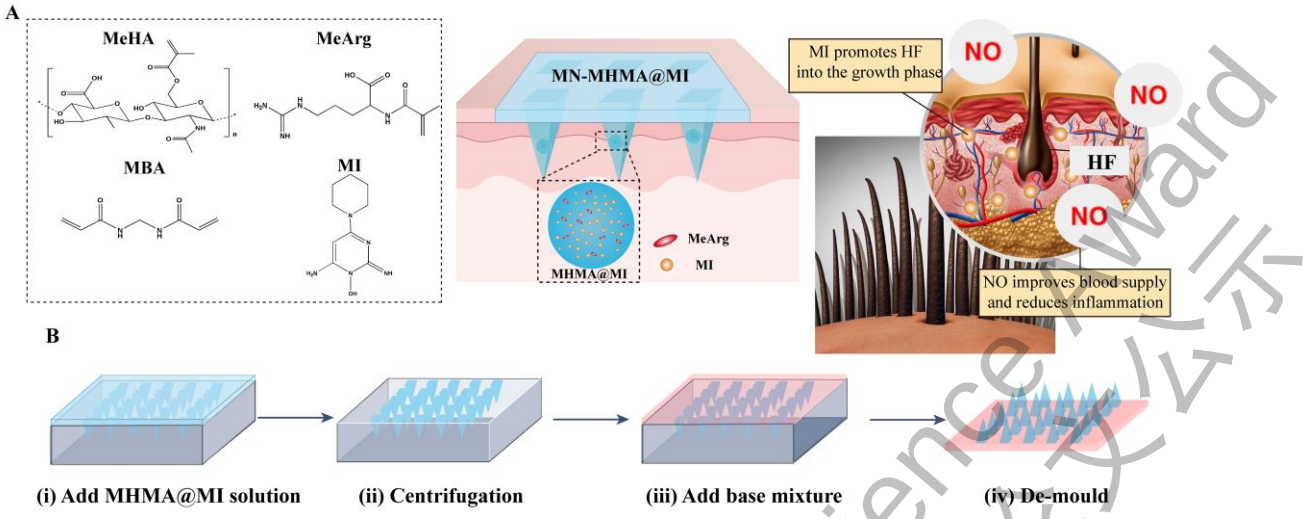

Scheme 2 Schematic diagram of the preparation process of hair-growth microneedles (MN-MHMA@MI) and its combination with minoxidil (MI) and NO donor (MeArg) for the treatment of androgenetic alopecia. (A) Constructing monomers and mechanism of action of MN-MHMA@MI. (B) The preparation process of MN-MHMA@MI.

2 Materials and Methods

2.1 Materials

Hyaluronic acid, arginine, methacrylic anhydride, minoxidil, N, N-methylene bisacrylamide (MBA), photoinitiator Irgacure 2959, ethanol, acetone, glacial acetic acid, testosterone, Texas-red fluorescent dye, polydimethylsiloxane (PDMS).

2.2 Animals

Male C57BL/6 mice, 8 weeks old

2.3 Preparation of main solutions

Acetate buffer (pH 2.5): Mix 25 mL of acetic acid solution with 200 mL of water, adjust the pH to 2.50 (±0.05) with NaOH (40% w/v), and finally adjust the volume to 250 mL with ultrapure water.

Sulfanilamide solution (Griess): Weigh 0.6 g of sulfanilamide into a 100 mL volumetric flask, add 40 mL of HCl (1 mol/L), and adjust the volume to 100 mL with ultrapure water.

Naphthyl ethylenediamine solution (NED): Weigh 0.6 g of NED into a 100 mL volumetric flask, add 40 mL of HCl (1 mol/L), and adjust the volume to 100 mL with ultrapure water.

2.4 Synthesis of methacryloylated hyaluronic acid

Dissolve 1.0g of HA in 50 mL of pure water at 4°C, add 0.8 mL of methacrylic anhydride (MA) dropwise, adjust the pH of the reaction solution to 8-9 with 5N NaOH, and stir for 24 hours at 4°C.

After the reaction is complete, precipitate the product in acetone, wash with ethanol, dissolve again in pure water, dialyze for 2 days, and lyophilize to obtain methacryloyl hyaluronic acid (MeHA).

2.5 Synthesis of methacryloylated arginine

Dissolve 2.0 g of arginine in a mixture of 8.5 mL of 1,4-dioxane and 20 mL of deionized water. Add 4.5 mL of triethylamine while stirring. Cool the mixture to 0 ℃, then add 3 mL of methacrylic anhydride dropwise for over 10 minutes. Stir the mixture at 25 ℃ for 24 hours. Precipitate the product in 400 mL of acetone, dissolve it in water, and precipitate again in acetone (**Fig. 1A**). Lyophilize to obtain methacryloyl arginine (MeArg) (**Fig. 1B**).

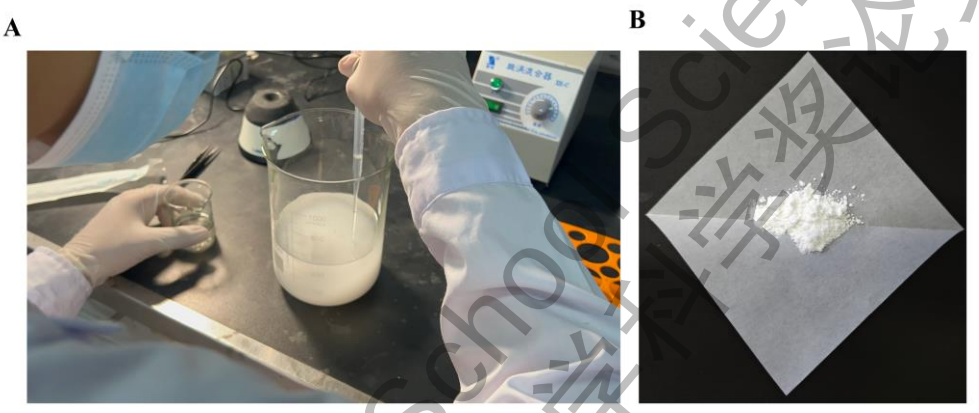

Fig. 1 (A) Acetone precipitation process. (B) Product after freeze-drying.

2.6 Preparation of nanogels

As shown in **Table 1**, mix the following materials in 1 ml of 0.3% acetic acid aqueous solution. Then expose the mixture to UV light for 60 seconds for crosslinking, and prepare nanogels (MHMA@MI). Measure the hydrated particle size and dynamic dispersion coefficient with a laser particle size analyzer. The screened particle size should be in the range of 400-600 nm, with a polydispersity index (PDI) of less than 0.3.

Table 1. Dosages of each component for formulation screenings

Materils（mg/mL）	Formulations				
	1	2	3	4	5
Minoxidil	2	2	2	2	2
MeHA	0	4	4	4	4
MeArg	4	0.5	1	0.5	0
MBA	0.6	0.6	0.6	1.2	0.6
Irgacure 2959	0.2	0.2	0.2	0.2	0.2

Additionally, after finalizing the formulation, perform NMR spectroscopy on the nanogels to confirm if cross-linking reactions have occurred and if covalent bonds have been formed

2.7 Detection of encapsulation efficiency of minoxidil in nanogels

Using HPLC detection methods, the amount of free minoxidil in the crosslinked system was measured to determine the encapsulation efficiency of the nano-gel MH-MA@MI for minoxidil (MI). Specifically, after crosslinking, the system was centrifuged using an ultrafiltration tube with a molecular weight cut-off of 300 KDa under the following conditions: 4000 rpm for 15 minutes. The free MI was centrifuged into the ultrafiltration outer tube, filtered through a 0.22 μm filter head, and then detected by the machine.

Preparation of the mobile phase: Aqueous phase: an aqueous solution containing 1% trifluoroacetic acid; Organic phase: methanol. After the mobile phase was prepared, it was filtered and degassed by ultrasonic treatment.

Chromatographic conditions: Flow rate: 1 mL/min; Elution conditions: Aqueous phase: Organic phase = 40:60; Injection volume: 20 μL; Column temperature: 30°C. A series of standard solutions with different concentrations were prepared by gradient dilution of the minoxidil standard solution. High-performance liquid chromatography (HPLC) was used for standard injection to obtain sample absorption peaks (peak area) and to plot the standard curve.

Detection was performed according to the above chromatographic detection method, and the standard curve was plotted based on the linear relationship between peak area (A) and drug concentration (C). The sample was prepared and detected according to the above method, and the measured peak area was substituted into the standard curve to calculate the amount of free MI in the sample. The encapsulation efficiency of MI in the formulation was then calculated using the following formula:

$$Encapsulation\ \text{efficiency}\% = \frac{C_t - C_f}{C_t} \times 100\%$$

Here, C_t represents the total amount of MI added; C_f represents the total amount of free MI.

2.8 Preparation and characterization of hair-growth microneedles

For the preparation of the microneedles: The PDMS microneedle mold is plasma cleaned, then 40 μL of MHMA@MI solution is applied to the PDMS microneedle mold and subjected to pressure treatment (0.3 MPa, 5 minutes), followed by drying in a fume hood. Another 40 μL of MHMA@MI solution is then applied to the mold, subjected to vacuum treatment (-0.1 MPa, 12 minutes), and dried again in a fume hood. Once completely dry, 11 μL of HA solution (0.5 g/mL) is applied to the PDMS microneedle mold, subjected to vacuum treatment (-0.1 MPa, 12 minutes), and dried in a fume hood for 3 hours until fully dry. The microneedles are then peeled off and stored in a desiccator for later use. The preparation process of MN-MI (microneedles loaded with minoxidil) is identical to that of MN-

MHMA@MI.

2.8.1 Detection of drug loading in hair-growth microneedles

Peel off and collect the tips of the MN-MHMA@MI microneedles, add 1 mL of ethanol (per patch), sonicate with a probe, filter through a 0.22 μm filter head, and then detect the MI content using the HPLC method described in section 2.7.1.

2.8.2 The amount of NO produced by hair-growth microneedles

The needle tips of MN-MHMA@MI were peeled off and collected, dissolved in 0.5 mL of UP water and H_2O_2 (200 μM), and placed in a shaker set at a speed of 100 rpm/min and a temperature of 37°C. After incubation for 6 hours, 50 μL of the obtained sample was taken and the NO content was detected using the Griess method.

NO standard curve preparation: Prepare a 10^{-4} mol/L $NaNO_2$ working solution and use acetate buffer (pH = 2.5) to prepare a series of concentrations: 10^{-6}, 2×10^{-6}, 5×10^{-6}, 7×10^{-6}, 10×10^{-6} mol/L. Then, add 200 μL of Griess reagent to the sample, gently shake, and react in the dark for 3 minutes. Continue by adding 50 μL of NED solution, gently shake, and react in the dark for 5 minutes.

Detection principle[21, 22]: NO^{2-} is a stable end metabolite of NO. Under acidic conditions, NO_2^- reacts with sulfanilamide in the Griess reagent to form a diazonium salt, which then reacts with N-(1-naphthyl) ethylenediamine (NED) to produce a magenta diazo dye. The absorbance of this magenta dye is measured at 540 nm using microplate reader to calculate the NO content in the solution (**Fig. 2**).

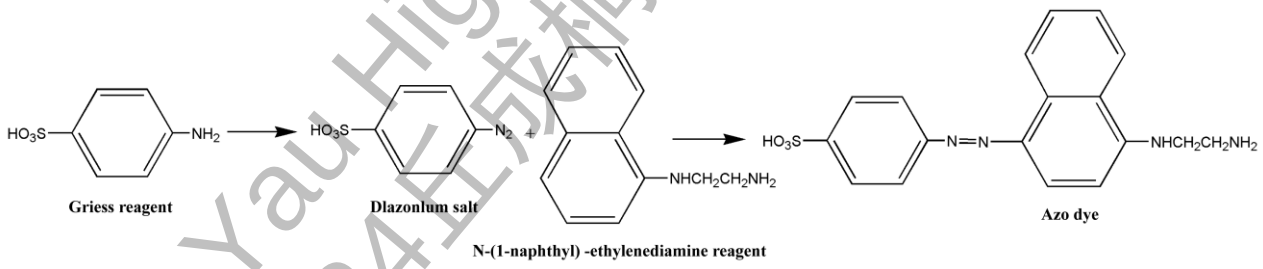

Fig. 2 Principle of NO Detection.

2.8.3 Morphological characterization of the microneedles

Using scanning electron microscopy (SEM), confocal laser scanning microscopy (CLSM), and optical sectioning microscopy to scan the morphology of microneedles, including assessing the integrity and tip morphology of the microneedles.

2.8.4 Evaluation of the mechanical properties of the microneedles

Using a force gauge (MARK-10) to measure the rupture force and rupture displacement of MN-

MI and MN-MHMA@MI, and recording the force-displacement curve.

2.8.5 Evaluation of the puncture efficiency of the microneedles

Attach the prepared MN-MHMA@MI microneedles (**Fig. 3A**) to the microneedle delivery injector device (**Fig. 3B**), press the MN-MHMA@MI onto the skin of male C57BL/6 mice for 3 minutes, and then remove the microneedle backing layer (**Fig. 3C**). Subsequently, euthanize the mouse and excise the skin from the application site. Stain the microneedle puncture sites with 30 μL of Coomassie Brilliant Blue for 5 minutes, then wash off the excess dye and observe under a microscope. The puncture efficiency of the microneedles is determined by the ratio of blue-stained holes to the total number of microneedles.

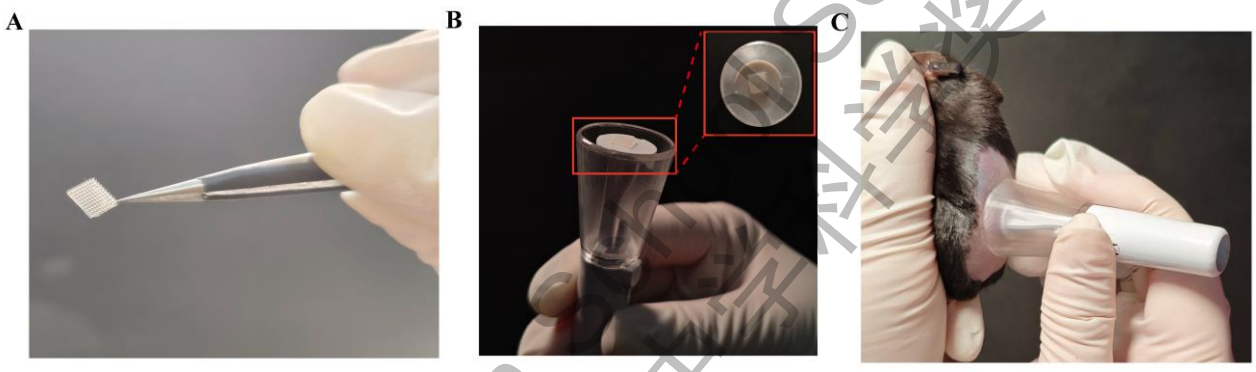

Fig. 3 (A) Image of the microneedles. (B) Diagram of the drug delivery injector device. (C) Microneedle drug delivery process.

2.8.6 Efficacy evaluation

Day 0: Shave the back skin of the mice with a hair clipper and perform a thorough hair removal treatment with depilatory cream. Randomly divide the mice into the following groups: Model, Minoxidil Solution (MI), Minoxidil Microneedle (MN-MI), and Nanogel Microneedle Loaded with Minoxidil (MN-MHMA@MI). Anesthetize all groups and apply a 0.5% testosterone solution to the depilated area, maintaining it for 20 minutes[23]. Apply the testosterone solution throughout the observation period to maintain the androgen-induced alopecia model.

Treatment Protocol: On Day 1, start treatment with different formulations for all groups except the Model groups. Administer treatment every three days for a total of 5 doses over 13 days. Specifically, MI tincture: Apply minoxidil solution to the hair loss area; MN-MI: Microneedles loaded solely with minoxidil were applied to the hair loss areas for 3 minutes; MN-MHMA@MI: Microneedles loaded with MN-MHMA@MI were applied to the hair loss areas for 3 minutes.

Efficacy Assessment: Throughout the observation period, mice were photographed on days 0, 18,

22, and 28 to monitor hair growth. On day 28, the mice from each group were euthanized, and their skin was harvested for hair follicle examination using a trichoscope (**Fig. 4A, B**). Additionally, skin samples were fixed and analyzed using HE staining and CD31 immunofluorescence staining to assess hair follicle conditions and angiogenesis.

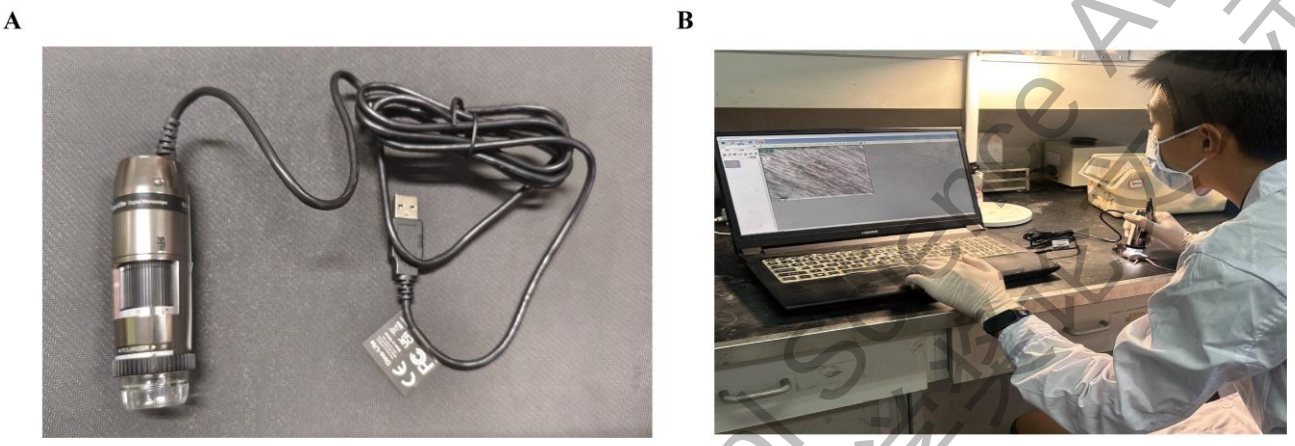

Fig. 4 (A) Diagram of the trichoscope device. (B) Imaging process using the trichoscope.

3 Results and discussion

3.1 Synthesis and characterization of methacarylated hyaluronic acid

The synthesis route of the methacarylated hyaluronic acid (MeHA) monomer is shown in Fig. 5A. Compared to the ^{1}H NMR spectrum of HA (Fig. 5B), the ^{1}H NMR spectrum of MeHA displayed characteristic peaks from the two hydrogens on the C = C bond. The chemical shifts (ppm) of each proton were as follows, denoted by δ: δ6.1 (s, 1H), 5.7 (s, 1H), 1.9 (s, 3H), 1.83 (s, 3H) (Fig. 1C). These values were consistent with theoretical expectations, and the spectrum showed no other impurity peaks, indicating the successful synthesis of a structurally accurate MeHA monomer that meets experimental requirements

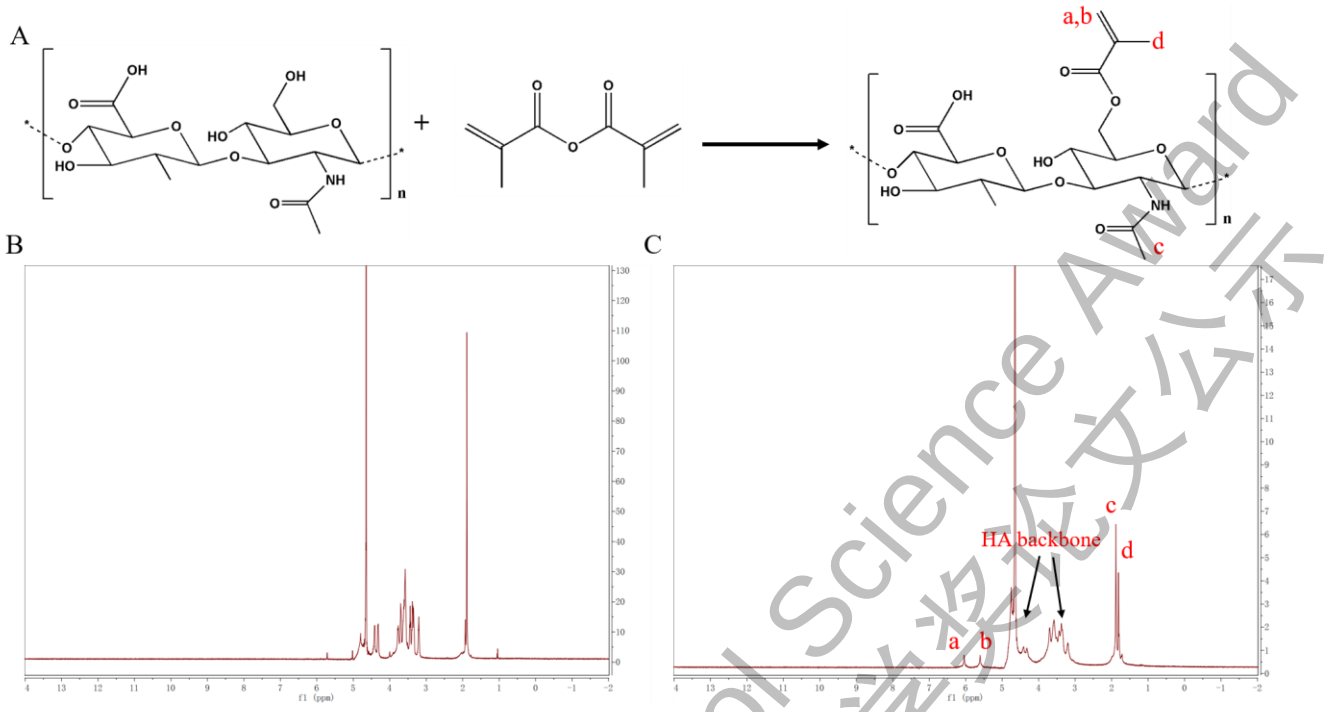

Fig.5 (A) Synthesis process of methacryloylamide-arginine (MeHA). (B) ^{1}H NMR spectrum of HA (C)1H NMR spectrum of MeHA (D2O, 400 MHz). ^{1}H NMR (400 MHz, D2O) δ6.1 (s, 1H), 5.7 (s, 1H), 1.9 (s, 3H), 1.8 (s, 3H), indicating the successful synthesis of MeHA.

3.2 Synthesis and characterization of methacarylated arginine

The synthesis route of the methacarylated arginine (MeArg) monomer is shown in Fig. 6A. Compared to the ^{1}H NMR spectrum of arginine (Arg) (Fig. 6B), the ^{1}H NMR spectrum of MeArg displayed characteristic peaks from the two hydrogens on the C = C bond. The chemical shifts (ppm) of each proton were as follows, denoted by δ: δ5.61 (s, 1H), 5.35 (s, 1H), 4.13 (dd, 1H), 3.09 (t, 2H), 1.83 (s, 3H), 1.81-1.59 (m, 2H), 1.56-1.46 (m, 2H) (Fig. 6C). These values were consistent with theoretical expectations, and the spectrum showed no other impurity peaks, indicating the successful synthesis of a structurally accurate MeArg monomer that meets experimental requirements.

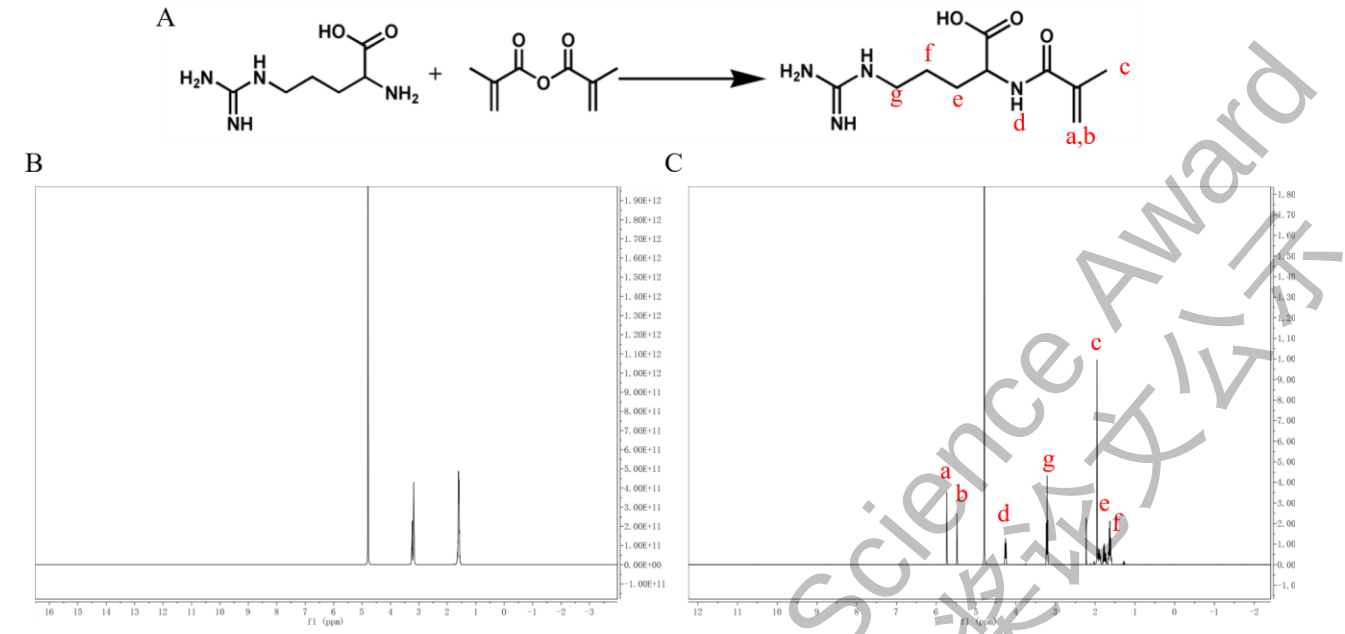

Fig.6 (A) Synthesis process of methacryloylamide-arginine (MeArg). (B) ^{1}H NMR spectrum of Arg (C)^{1}H NMR spectrum of MeArg (D2O, 400 MHz). ^{1}H NMR (400 MHz, D2O) δ5.61 (s, 1H), 5.35 (s, 1H), 4.13 (dd, 1H), 3.09 (t, 2H), 1.83 (s, 3H), 1.81-1.59 (m, 2H), 1.56 -1.46 (m, 2H), indicating the successful synthesis of MeArg.

3.3 Synthesis and Characterization of Nanogels

Laser diffraction particle size analysis measures particle size by directing a laser beam through a sample. The particles scatter the laser light, and the angle of this scattering is related to the particle size. The instrument collects and analyzes these scattered light signals using specific algorithms to calculate the particle size distribution. The Polydispersity Index (PDI) reflects the uniformity of particle size and is a crucial indicator of particle size characterization.

According to Section 2.6, five different formulations were prepared, with their corresponding particle sizes and PDIs shown in **Fig. 7A**. Notably, the cross-linked formulation 3 exhibited a particle size of 522.9 nm and a PDI of 0.144, demonstrating that the monodisperse nanogel (MHMA@MI) with a uniform particle size was successfully prepared, meeting the criteria for targeting hair follicles. Additionally, the high encapsulation efficiency of minoxidil in the nanogel is vital for the formulation's success. HPLC analysis revealed that the nanogel encapsulates minoxidil with an efficiency of 87.64% (**Fig. 7B**), indicating a successful formulation with high minoxidil loading.

Furthermore, NMR results (**Fig. 7C**) showed that peaks at 6.1 ppm and 5.7 ppm (MeHA), 5.61 ppm and 5.35 ppm (MeArg), and 5.8 ppm and 6.25 ppm (MBA) disappeared, signifying the complete consumption of the double bonds and the successful completion of the polymerization reaction, resulting in MHMA. These findings confirm that we have synthesized an MHMA nanogel with an approximate particle size of 500 nm, uniform particle size, and high minoxidil encapsulation efficiency.

A

Formulations	Size (nm)	PDI
1	2197	1.000
2	522.9	0.144
3	941.0	1.000
4	906.9	0.806
5	294.5	0.600

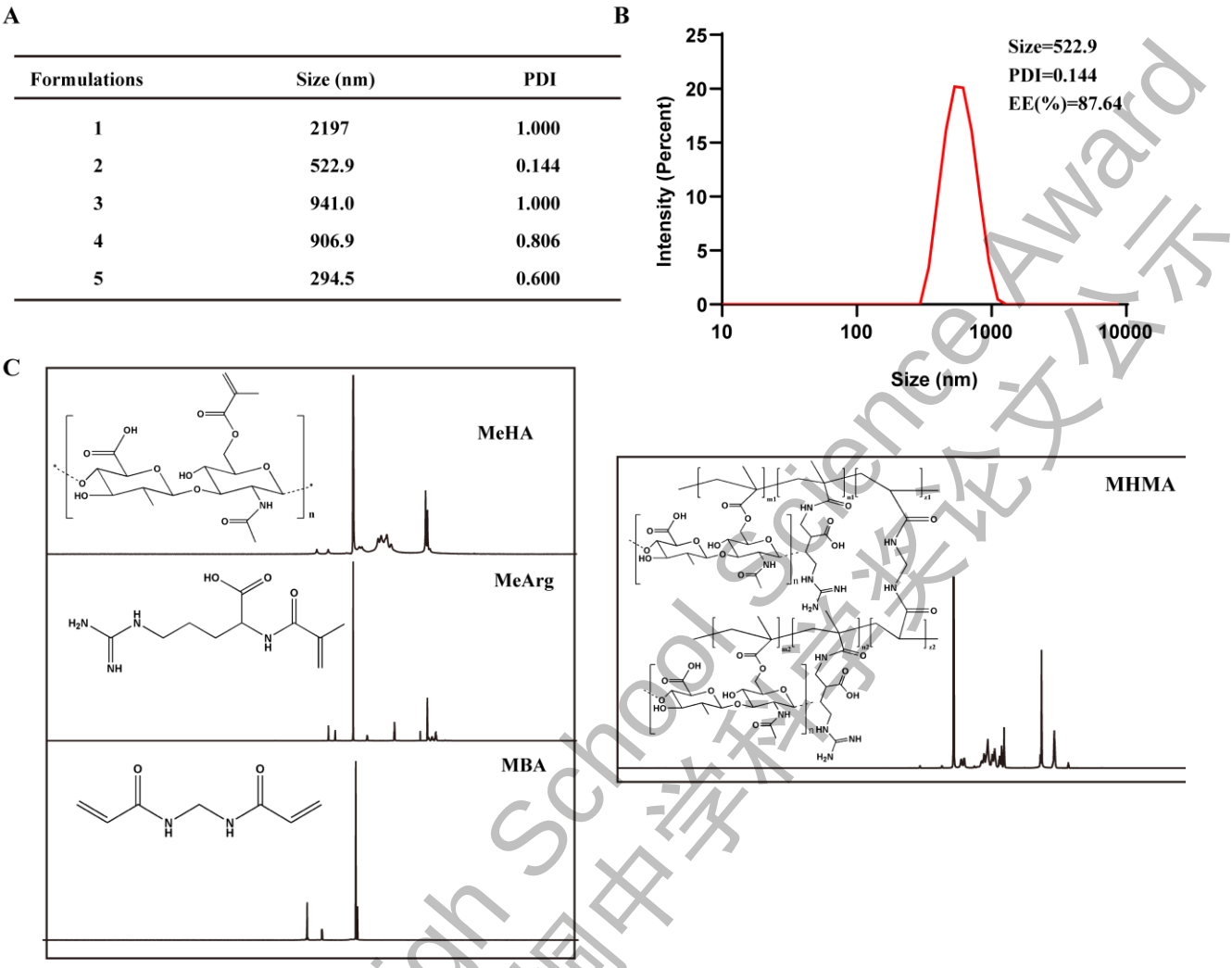

Fig. 7 (A) Formulation screening of nanogels, including particle size and Polydispersity Index (PDI) results. (B) Particle size distribution and encapsulation efficiency of MHMA. (C) ^{1}H NMR spectrum of MeHA, MeArg, MBA and MHMA.

3.4 Fabrication and Characterization of microneedle

The preparation method for two types of microneedles were similar: MI or MHMA@MI was filled into PDMS molds under reduced pressure and then dried. Subsequently, HA was further filled into the PDMS molds to form the final microneedle patches. Analysis of stereomicroscope images (**Fig. 8A**) and scanning electron microscope images (**Fig. 8B**) demonstrated that both microneedle types maintained intact morphology with sharp tips and heights exceeding 700 micrometers. Additionally, substituting texas red dye for minoxidil during microneedle preparation and scanning with a confocal microscope (**Fig. 8C**) revealed uniform drug distribution throughout the microneedles, which is beneficial for effective drug delivery.

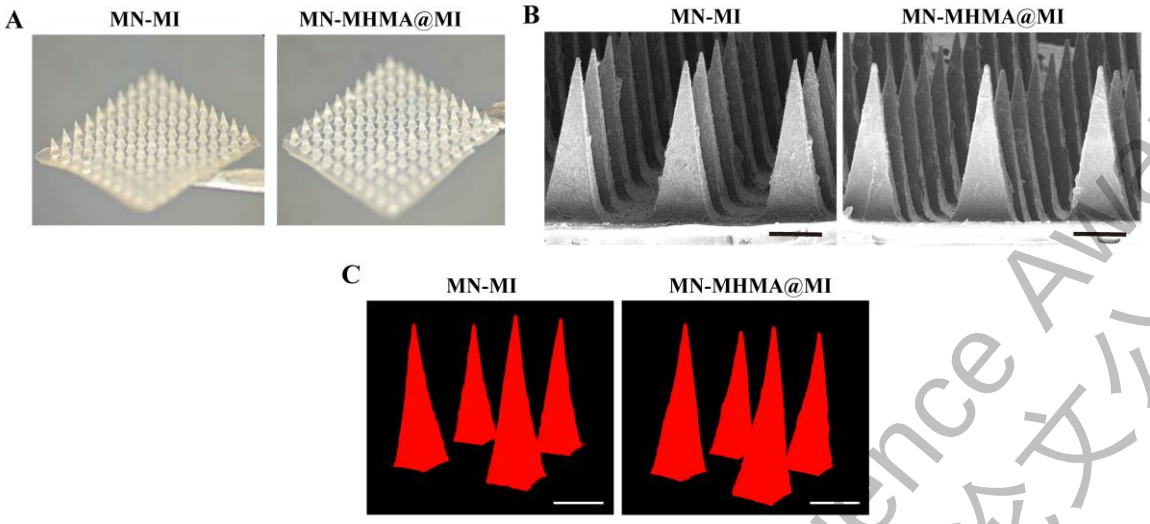

Fig. 8 (A) Stereomicroscope images of the two types of microneedles. (B) Scanning electron microscope images of the two types of microneedles, scale bar = 200 μm. (C) Confocal microscope images of the two types of microneedles, characterized using texas red dye instead of minoxidil, scale bar = 200 μm.

Compared to traditional formulations such as tinctures, microneedles offer a significant advantage in terms of patient compliance due to their painless delivery method, which is preferable to injections. However, adequate mechanical strength is essential for effective drug delivery via microneedles. We evaluated the mechanical properties of individual microneedles by measuring the break force-displacement curves (**Fig. 9A, B**). Further analysis of these curves yielded data on break displacement and break force. Statistical analysis demonstrated that the incorporation of nanogel significantly improved the mechanical performance of MN-MHMA@MI compared to MN-MI, with performance metrics well above the 0.058 N/needle threshold required for skin penetration (**Fig. 9C, D**). These findings indicate that the microneedles developed using our designed nanogel exhibit optimal mechanical performance.

To further assess the practical piercing efficiency of the microneedles, we applied them to the dorsal skin of mice using a custom ejector for 3 minutes. Following removal, the skin was stained with evans blue for 3 minutes. The results demonstrated that both types of microneedles achieved 100% piercing efficiency, effectively penetrating the skin (**Fig. 9E**).

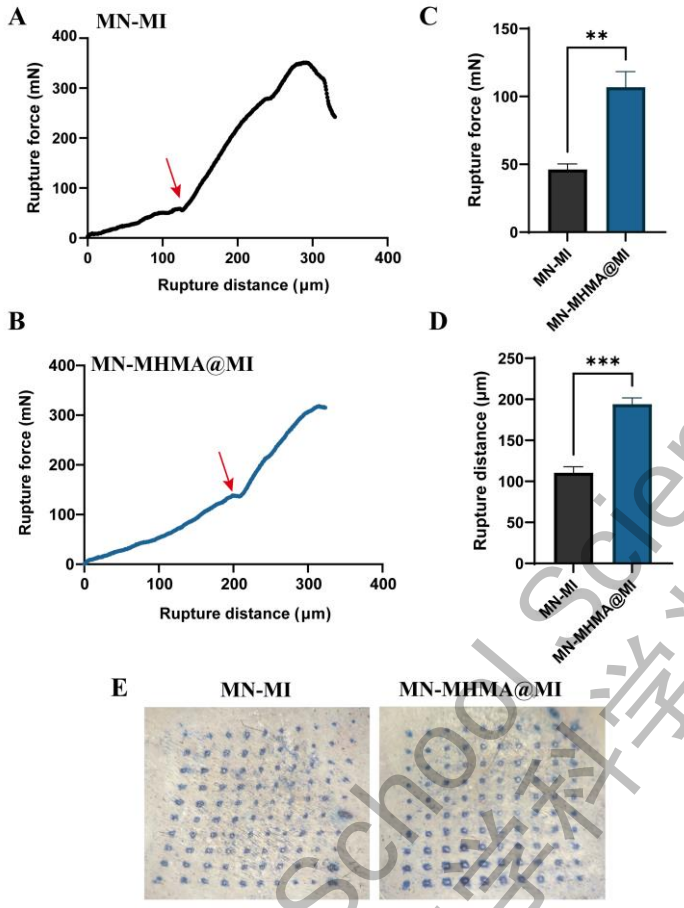

Fig. 9 (A, B) Rupture force-distance curves for the two types of microneedles. (C, D) Rupture force and rupture distance for the two types of microneedles. (E) Piercing efficiency of the two types of microneedles on the dorsal skin of C57BL/6 mice, as assessed by evans blue staining. Data are represented as mean ± SEM (n=4). Student's t-test analysis in Graphpad Prism9.0. Levels of significant differences were expressed as follows, *P < 0.05, **P < 0.01, ***P < 0.001, ****P < 0.0001.

Finally, HPLC analysis of the drug loading capacity for minoxidil in the two types of microneedles showed that the drug load was 124.9 μg/patch for one type and 127.92 μg/patch for the other, with no significant difference between them (**Fig. 10A**). Additionally, the amount of arginine-loaded MN-MHMA@MI that released NO was 0.78 μM/patch (**Fig. 10B**). All these results demonstrate the successful preparation of two types of minoxidil-loaded microneedles.

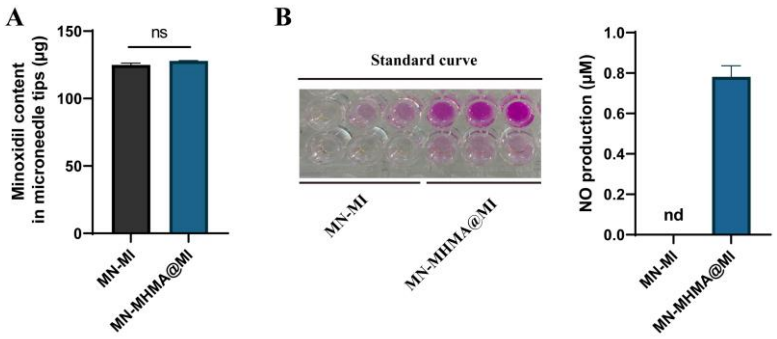

Fig. 10 (A) Amount of minoxidil loaded in the two types of microneedles. (B) Plate bottom images of NO detection and the amount of NO released from MN-MHMA@MI loaded with arginine. Data are represented as mean ± SEM (n=3). Student's t-test analysis in Graphpad Prism9.0. Levels of significant differences were expressed as follows, *P < 0.05, **P < 0.01, ***P < 0.001, ****P < 0.0001.

3.5 In vivo pharmacodynamic studies

Hair growth is characterized by a cyclical nature. To visually observe hair follicle (HF) development, the C57BL/6 mouse is commonly used in alopecia research. This is because the skin color of C57BL/6 mice is closely linked to the growth cycle of their hair follicles. Hair follicles contain melanocytes, and their growth is synchronized with melanocyte activity. During the active growth phase of hair follicles, melanocytes begin synthesizing and secreting melanin, resulting in darker skin. When hair follicle growth ceases and transitions to the resting phase, melanin production by melanocytes stops, and the skin gradually returns to a pink color. Thus, changes in skin color can indicate the growth phase of the hair follicles. For our experiments, we selected 8-week-old C57BL/6 mice. At this age, the skin follicles have completed their development and have transitioned from the growth phase to the resting phase, causing the skin to change from black to pink. Upon external stimuli such as hair removal, the hair follicles re-enter the growth phase, with renewed and comprehensive activation of follicle growth, leading to a subsequent change in skin color[23, 24].

In this experiment, an androgenetic alopecia (AGA) model in mice was established by applying a testosterone solution to the depilated area on the back of the mice, as previously described (section 2.8). 8-week-old male C57BL/6 mice were randomly divided into four groups (n=4) and depilated on the back on day 0. Different treatments were administered on days 1, 4, 7, 10, and 13, with daily application of 0.5% testosterone solution to maintain the AGA model (**Fig. 11A**). The regrowth of hair in the depilated area over time is shown in **Fig. 11B-E**. In the testosterone-treated group (Model group), hair regrowth in the depilated area was significantly inhibited. By day 18, the skin on the back remained pale pink without any darkening, and no signs of hair regrowth were observed throughout the observation period. In contrast, MI tincture, MN-MI, and MN-MHMA@MI groups showed some new hair growth around day 18, with MN-MHMA@MI exhibiting the most extensive coverage and

significant pigmentation, indicating that the hair follicles had entered the growth phase. By day 28, the MN-MHMA@MI group showed the best hair regrowth, with the largest hair coverage area.

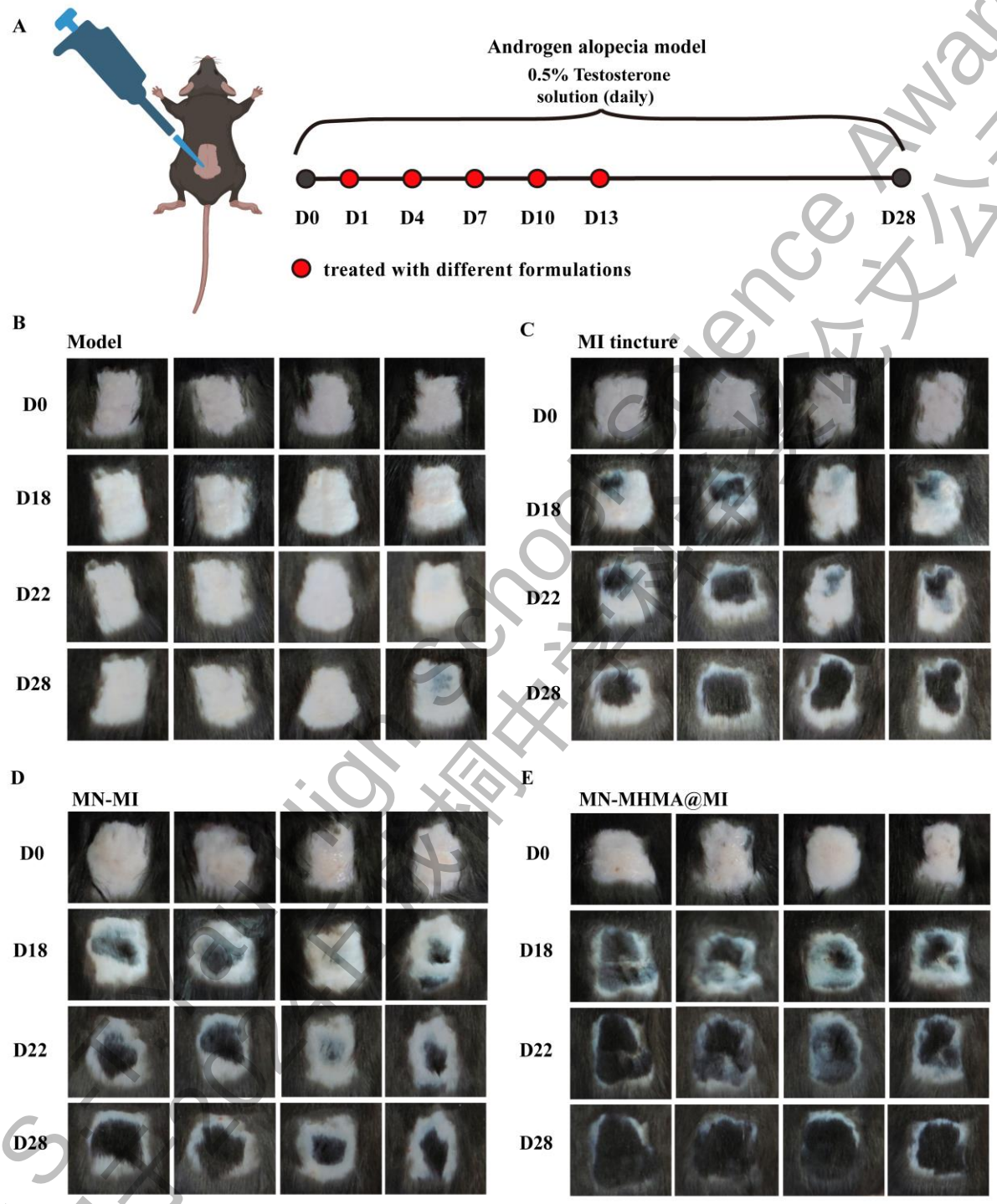

Fig. 11 (A) Pharmacodynamic animal experimental protocol. (B-E) Photographic results of hair regrowth on the backs of mice in the Model, MI tincture, MN-MI, and MN-MHMA@MI groups, taken on days 0, 18, 22, and 28, respectively. (n=4).

A trichoscope is a crucial diagnostic tool for hair loss, offering significant value in diagnosing,

grading, and assessing the efficacy of treatments for androgenetic alopecia. It facilitates a clearer observation of hair follicle openings, hair shafts, and the surrounding skin (**Fig. 12A**). As shown in **Fig. 12B**, the MN-MHMA@MI group demonstrated uniformly distributed hair with neatly aligned roots and normal morphology, displaying significant differences compared to the Model, MI tincture, and MN-MI groups.

Fig. 12 (A) Schematic of trichoscope imaging. (B) Observation results of hair regrowth on the backs of mice in the Model, MI tincture, MN-MI, and MN-MHMA@MI groups using the trichoscope on day 28. (n=4).

To further assess the condition of the skin and hair follicles in the mice[25, 26], we conducted Hematoxylin and Eosin (HE) staining on skin samples from the drug application areas of each group. The results are presented in **Fig. 13A**. On day 28, hair follicles (HFs) in the Model group remained in the resting phase. In the MI tincture group, only a few hair follicles had transitioned to the growth

phase. In contrast, the MN-MI and MN-MHMA@MI groups exhibited hair follicles advancing to the growth phase, with increased follicle depth. Notably, the MN-MHMA@MI group showed hair follicle bulbs with increased volume and accompanying melanin production. Additionally, CD31 a specific marker for endothelial cells, reflects the extent of angiogenesis. The CD31 immunofluorescence staining results (**Fig. 13B**) showed that the MN-MHMA@MI group exhibited prominent red fluorescence, indicating that the nanogel co-loaded with NO donors (MeArg) and minoxidil effectively promoted CD31 expression and enhanced angiogenesis around the hair follicles.

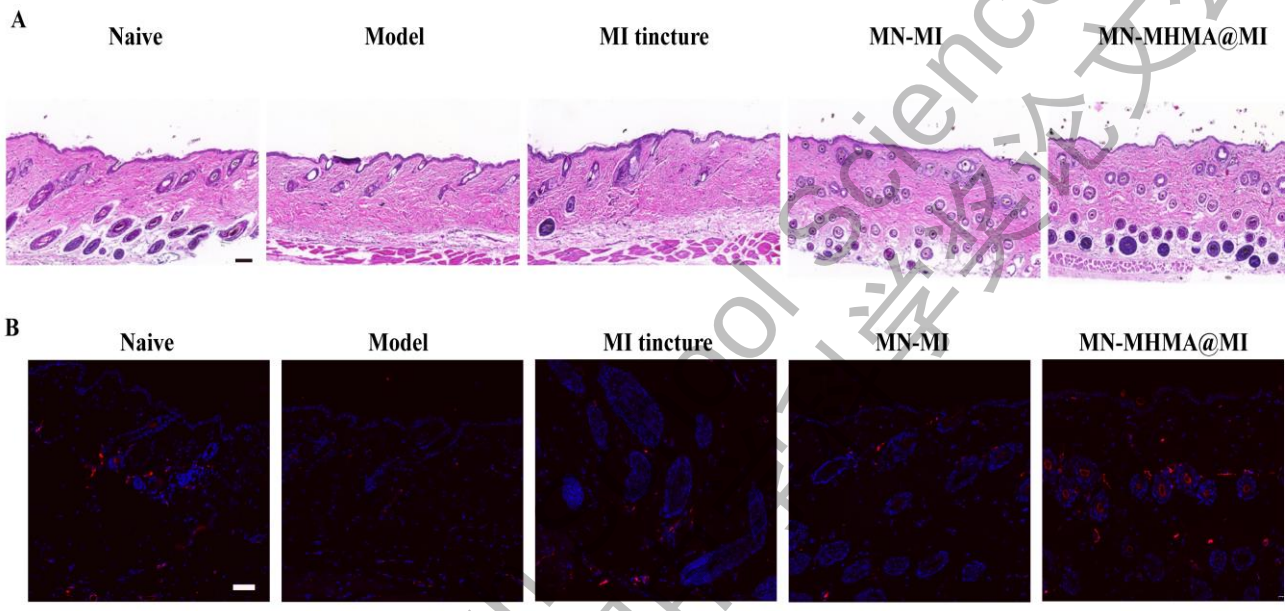

Fig. 13 (A) Representative HE staining images of the back skin from naïve, model, MI-tincture, MN-MI, and MN-MHMA@MI groups of mice, Scale bar =100 μm. (B) Representative CD31 immunofluorescence images of the back skin from the naïve, model, MI-tincture, MN-MI, and MN-MHMA@MI groups of mice, Scale bar =50 μm.

4 Conclusion

In summary, we developed a nanogel capable of high encapsulation of minoxidil through a straightforward chemical modification by covalently polymerizing an NO donor arginine. This was achieved via a simple photopolymerization reaction. Furthermore, we utilized this nanogel to fabricate microneedles with excellent mechanical properties. The microneedle material used in this study is hyaluronic acid (HA), a safe and biocompatible injectable excipient. The microneedles prepared in this study allow drug delivery with just a 3-minute application, enhancing patient compliance while minimizing the potential risk of skin irritation. Additionally, compared to commercial minoxidil tincture, these microneedles contain no organic solvents, significantly reducing the dosage of minoxidil and further improving safety. By encapsulating minoxidil in soluble microneedles using a gentle and

simple method, with an encapsulation efficiency exceeding 80%, we achieved co-delivery of minoxidil and the NO donor through the skin. The microneedles effectively delivered minoxidil and, with the aid of NO, effectively stimulated hair follicles to enter the growth phase, promoted angiogenesis and significantly enhanced hair growth, thereby achieving optimal therapeutic outcomes.

5 References

1. Zhou, Y. et al. Advances in microneedles research based on promoting hair regrowth. *Journal of Controlled Release* **353**, 965-974 (2023).
2. Inui, S. & Itami, S. Molecular basis of androgenetic alopecia: From androgen to paracrine mediators through dermal papilla. *Journal of Dermatological Science* **61**, 1-6 (2011).
3. Gu, Y., Bian, Q., Zhou, Y., Huang, Q. & Gao, J. Hair follicle-targeting drug delivery strategies for the management of hair follicle-associated disorders. *Asian Journal of Pharmaceutical Sciences* **17**, 333-352 (2022).
4. Wang, R. et al. PROTAC Degraders of Androgen Receptor-Integrated Dissolving Microneedles for Androgenetic Alopecia and Recrudescence Treatment via Single Topical Administration. *Small Methods* **7**, 2201293 (2023).
5. Rabbani, P. et al. Coordinated Activation of Wnt in Epithelial and Melanocyte Stem Cells Initiates Pigmented Hair Regeneration. *Cell* **145**, 941-955 (2011).
6. Heymann, W.R. The inflammatory component of androgenetic alopecia. *Journal of the American Academy of Dermatology* **86**, 301-302 (2022).
7. Saleem, K., Siddiqui, B., ur.Rehman, A., Taqi, M.M. & Ahmed, N. Exploiting Recent Trends in the Treatment of Androgenic Alopecia through Topical Nanocarriers of Minoxidil. *AAPS PharmSciTech* **23**, 292 (2022).
8. Messenger, A.G. & Rundegren, J. Minoxidil: mechanisms of action on hair growth. *British Journal of Dermatology* **150**, 186-194 (2004).
9. Millar, S.E. Molecular Mechanisms Regulating Hair Follicle Development. *Journal of Investigative Dermatology* **118**, 216-225 (2002).
10. Namazi, M.R. Nitric oxide donors as potential additions to anti-alopecia areata armamentarium. *Inflammation Research* **52**, 227-229 (2003).
11. Xing, H. et al. Nitric oxide synergizes minoxidil delivered by transdermal hyaluronic acid liposomes for multimodal androgenetic-alopecia therapy. *Bioactive Materials* **32**, 190-205 (2024).
12. Yang, T., Zelikin, A.N. & Chandrawati, R. Progress and Promise of Nitric Oxide-Releasing Platforms. *Advanced Science* **5**, 1701043 (2018).
13. Wan, M. et al. Bio-inspired nitric-oxide-driven nanomotor. *Nature Communications* **10**, 966 (2019).
14. Yazdani-Arazi, S.N., Ghanbarzadeh, S., Adibkia, K., Kouhsoltani, M. & Hamishehkar, H. Histological evaluation of follicular delivery of arginine via nanostructured lipid carriers: a novel potential approach for the treatment of alopecia. *Artificial Cells, Nanomedicine, and Biotechnology* **45**, 1379-1387 (2017).
15. Salim, S. & Kamalasanan, K. Controlled drug delivery for alopecia: A review. *Journal of Controlled Release* **325**, 84-99 (2020).

16. Schneider, M.R., Schmidt-Ullrich, R. & Paus, R. The Hair Follicle as a Dynamic Miniorgan. *Current Biology* **19**, R132-R142 (2009).
17. Correia, M. et al. Nanotechnology-based techniques for hair follicle regeneration. *Biomaterials* **302**, 122348 (2023).
18. Mishra, P. et al. Potential of nanoparticulate based delivery systems for effective management of alopecia. *Colloids and Surfaces B: Biointerfaces* **208**, 112050 (2021).
19. Patzelt, A. et al. Selective follicular targeting by modification of the particle sizes. *Journal of Controlled Release* **150**, 45-48 (2011).
20. Matos, B.N. et al. Follicle-Targeted Delivery of Betamethasone and Minoxidil Co-Entrapped in Polymeric and Lipid Nanoparticles for Topical Alopecia Areata Treatment. *Pharmaceuticals* **16**, 1322 (2023).
21. Goshi, E., Zhou, G. & He, Q. Nitric oxide detection methods in vitro and in vivo. *Medical Gas Research* **9** (2019).
22. Rahat, M.A. & Hemmerlein, B. Macrophage-tumor cell interactions regulate the function of nitric oxide. *Frontiers in Physiology* **4** (2013).
23. Yuan, A. et al. Ceria Nanozyme-Integrated Microneedles Reshape the Perifollicular Microenvironment for Androgenetic Alopecia Treatment. *ACS Nano* **15**, 13759-13769 (2021).
24. Müller-Röver, S. et al. A Comprehensive Guide for the Accurate Classification of Murine Hair Follicles in Distinct Hair Cycle Stages. *Journal of Investigative Dermatology* **117**, 3-15 (2001).
25. Flores, A. et al. Lactate dehydrogenase activity drives hair follicle stem cell activation. *Nature Cell Biology* **19**, 1017-1026 (2017).
26. Gao, S.-Q. et al. Co-delivery of deferoxamine and hydroxysafflor yellow A to accelerate diabetic wound healing via enhanced angiogenesis. *Drug Delivery* **25**, 1779-1789 (2018).

6 Acknowledgement

Topic selection and research background of this research

The topic of this research was generated from the independent thinking of Xueyang Wang, based on the severe hair loss his father has been suffering. After consulting clinical doctors, under the guidance of his chemistry teachers Xuojie Qu and Chunyan He, he finished the project design, experiments, data processing and paper writing. Of note, he synthesized photopolymerizable materials and successfully applied them for the better treatment of hair loss.

The relationship between instructors and the students and whether the guidance is paid

The instructors Xiaojie Ju and Chunyan He are the chemistry teachers of Xueyang Wang. Mrs. Ju and Mrs. He guided the study design, experiments and manuscript writing for free.

Data completed with the assistance of others

Shu Wang and Shuping Zheng, technicians from the Analytical & Testing Center of Sichuan University, assisted the characterization of hair-growth microneedle materials by nuclear magnetic resonance (NMR) and scanning electron microscope (SEM), which were the entrusted testing service.

致谢

- **论文的选题来源、研究背景**

本论文的选题源于王雪扬同学的自主思考。针对困扰父亲的严重脱发问题，王雪扬在咨询临床医生后，在化学老师巨晓洁和何春燕的指导下，立足化学学科的聚合物化学领域，完成了项目设计、实验、数据处理和论文撰写工作。通过合成两种光聚合材料（MeHA 和 MeArg），并利用自聚合方法制备出纳米凝胶（MHMA@MI），成功实现了一氧化氮供体与米诺地尔的共载。进一步地，制备了装载纳米凝胶的增发微针（MN-MHMA@MI），并在雄激素脱发小鼠模型中成功实现了毛发再生，为临床雄激素脱发的治疗提供了一个具有前景的新方向。

- **指导老师与学生的关系，在论文写作中的作用，及指导是否有偿**

指导老师巨晓洁和何春燕是王雪扬的化学老师，巨老师和何老师完成了论文的修改与优化。两位老师无偿指导了研究设计、实验和论文写作。

- **他人协助完成的研究成果**

四川大学分析测试中心的技术人员王书和郑淑萍协助完成了光聚合材料（MeHA、MeArg 和 MBA）及纳米凝胶（MHMA@MI）的核磁共振（HNMR）表征，以及增发微针（MN-MHMA@MI）的扫描电子显微镜（SEM）表征，属于委托测试服务。

- **不同环节遇到的困难及解决问题的经过**

MeHA 合成过程：在合成 MeHA 的过程中，由于没有很好的控制反应过程的 pH 为 8-9，导致无法实现透明质酸的甲基丙烯酰化。为了解决上述问题，王雪扬在巨老师的指导下，将 pH 剂的探头插入反应液中，实时监控反应液的 Ph 变化，采用氢氧化钠控制反应 pH 为 8-9 之间，成功合成了甲基丙烯酰化的透明质酸（MeHA）。

MeArg 合成过程：MeArg 的纯化过程采用了丙酮沉淀法。最初，由于丙酮加入量不足以及沉淀时间不够，导致最终产物的产量较低。为解决这些问题，通过进一步的文献调研和与两位老师的讨论，决定将丙酮的用量提高至反应液体积的 10 倍以上，并将沉淀时间延长至 12 小时。这些调整有效地提高了产物的产量。

小鼠毛发生长情况的评估：在药效评估阶段，通过毛发镜可以观察到每一只小鼠的毛发的生长情况，但是难以对各组间的毛发生长进行统计学分析。在四川省天府中学生英才计划的培育下，王雪扬同学基于他在编程方面的基础，在四川大学计算机学院赵启军教授的指导下，正在试图用图像识别的手段解决上面的难题。

参赛学生简历

姓名：王雪扬

获奖情况：

1. 2024 年入选四川省天府中学生英才计划
2. 2023 年成都市高新区第三届“引航杯”初中化学实践大赛三等奖
3. 2024 年美国 USACO 信息学竞赛银级

地址：四川大学附属中学，成都，610041，中国

电话：17713637479

邮箱：Aidenwang26@hotmail.com

指导老师简历

姓名：巨晓洁

职称：教授

地址：四川大学化学工程学院，成都，610065，中国

电话：13880649216

邮箱：juxiaojie@scu.edu.cn

姓名：何春燕

职称：一级教师

地址：四川大学附属中学，成都，610021，中国

电话：17360663006

邮箱：564942256@qq.com